Atom recoil during coherent light scattering from many atoms

F. Robicheaux[1,2,*] and Shihua Huang[1]
[1]*Department of Physics and Astronomy, Purdue University, West Lafayette, Indiana 47907, USA*
[2]*Purdue Quantum Center, Purdue University, West Lafayette, Indiana 47907, USA*

(Received 14 November 2018; published 9 January 2019)

The recoil momentum and energy of ultracold atoms is studied for situations where collective scattering or emission of photons is important. Effects due to the dipole-dipole interaction are emphasized. For two and many atoms confined in optical traps, calculations of the energy and momentum with respect to atomic separation are performed. When the atomic separation is comparable to or larger than the transition wavelength, the ultracold atoms' recoil energy depends mainly on collective spontaneous decay rather than forces from the cooperative frequency shift. Calculations for a laser pulse reflecting from an atomic array suggest that the recoil energy of atoms can be substantially larger than might be expected from an independent atom picture.

DOI: 10.1103/PhysRevA.99.013410

I. INTRODUCTION

The study of collective dipole interactions has been an active field for many decades. The original investigation in Ref. [1] predicted how several atoms within a wavelength could decay coherently. This concept has been widely explored (a sample of results includes Refs. [2–13] investigating a wide variety of topics including superradiance, subradiance, collective Lamb shift, etc.). One of the interesting avenues for collective effects are when the atoms are in an array because the uniform spacing lends itself to a buildup of coherence between the atomic states and the radiation field [14–21]. One of the possible applications of photons interacting with atom arrays involves quantum information [21–24]. Another interesting scenario arises through the observation that a single atom layer can act as a perfect mirror due to the collective dipole-dipole interaction as noted in Ref. [16] and extended in Ref. [17]. This perfect reflection as well as chiral quantum optics of the array in Ref. [24] promises the control of light fields using small arrays of atoms.

Among these efforts with atom arrays, especially those related to quantum information or to control of light, a potential concern to be considered is the entanglement between the internal and positional degrees of freedom of the cold atoms or the entanglement between the photon and atomic position degrees of freedom. The atoms' motion can then affect the evolution of the atoms' internal states and the interaction of subsequent photons with the atom array. At the simplest level, this leads to the recoil of an atom, e.g., Ref. [25]. Atomic recoil has been investigated in many situations, e.g., cases where the recoil changes the interaction with light, Refs. [26–28] among many possible cases. As another example, the collective atomic recoil laser (CARL) [29,30] technique uses the atoms' recoil as a mechanism for the amplification of the laser field. Other situations have also involved the atom motion, e.g., the self-organized cavity, utilize the collective dipole-dipole interaction of ultracold atoms coupled in a cavity as a friction force to form the atoms into patterns [31–35]. In addition, the radiation force and pressure on the gas center of mass in a cooperative scattering process of cold atomic ensembles has been investigated [36,37]. The dipole-dipole shifts and decay rates of cold atomic ensembles modulated through quantized atomic motion has been calculated [38].

In previous theoretical treatments, the atoms are either fixed in space (for a patterned grid) or integrated over space (for dense clouds) to simulate the evolution of internal states of the atoms or properties such as the scattered electric field. The main goal of this paper is to understand how a photon interacting with or reflecting from an array of atoms can lead to recoil momentum and energy for the atoms, especially when collective scattering is important.

The basic idea is illustrated in Fig. 1. Atoms are assumed trapped in an array of far off resonance traps [39,40] near their motional ground state and all in their electronic ground state. A photon is incident on the array, Fig. 1(a). During the scattering, the photon is temporarily absorbed, which leads to a collective, singly excited state with each atom's recoil entangled with its excitation, Fig. 1(b), because the photon has momentum. At a later time, the photon emerges and the different atoms can have different recoil directions. We will be investigating the case where each atom's vibrational period is much larger than the excited-state lifetime and the duration of the incident laser pulse. In this case, each atom's individual trap can be ignored during these steps because they happen much more quickly than the vibrational period. (This can be thought of as the impulse limit of the photon interaction.) Just after the photon emerges, the average change of momentum of all the atoms must equal minus the change in the photon momentum. However, it is not obvious how individual atoms recoil when the dipole-dipole interactions are important. For example, if the recoil is spread over several atoms, then the recoil energy would be substantially smaller than for a single atom. Recently, two papers [41,42] have addressed aspects of the recoil of atoms in arrays but in the opposite time limit

*robichf@purdue.edu

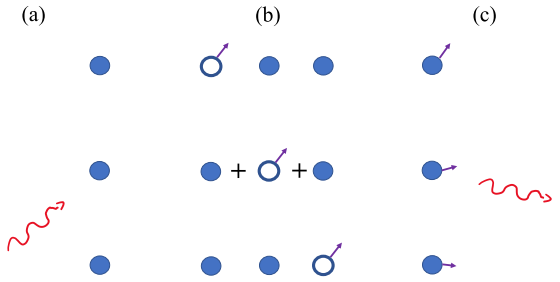

FIG. 1. A drawing of the process under consideration. Atoms in their electronic ground state are indicated by filled circles while electronically excited atoms are indicated by empty circles. The red, wavy arrows indicate the incoming and outgoing photon. The purple arrows indicate nonzero average momentum. (a) Three atoms in their electronic and motional ground state before absorbing a photon. (b) The single excitation and recoil due to photon absorption gives a superposition of three states. During this step, the atoms also interact through the dipole-dipole interaction. (c) After the photon is reemitted, the different atoms have different amounts of recoil. The average recoil momentum equals the change in the photon momentum but the average recoil energy might be larger or smaller than for a single atom.

so that the atomic vibrations are important. In this limit, they have found interesting collective behavior of the atoms.

In this paper, the collective recoil of an array of cold atoms in a collective scattering process is studied using master equations. The spatial dependence of the collective Lamb shift and the collective spontaneous decay both contribute to the atoms' recoil energy for small separations whereas the collective decay dominates for large separations. The contribution to the recoil energy and momentum from the spatial distribution of the atoms is relatively small for typical atomic trapping frequencies. Calculations with various size two-dimensional (2D) grids indicate that the recoil energy converges to a finite, nonzero result when the number of photons per unit grid area is constant. For a perfectly reflected photon, one might expect that the recoil energy would be $4E_r$ where $E_r = \hbar^2 k^2/(2M)$ because an atom would have a recoil of $2\hbar k$. If the photon momentum is distributed over several atoms in the collective reflection, then one would expect the recoil energy to be less than $4E_r$. There are cases described below where the recoil energy is larger than the expected value and, in one case, is $\sim 2\times$ larger than expected for perfect reflection. The difference between these outcomes can be very important because the recoil energy can be close to the energy spacing of an atom trap. For example, a 795 nm photon leads to $E_r \sim 0.2\,\mu$K for Rb whereas the energy spacing in a 20 kHz trap is $\sim 1\,\mu$K. Therefore, the difference between a recoil less than $4E_r$ or $2\times$ larger can be very important for exciting modes of the atom trap.

Section II describes the methods used for the calculations. Section III describes the results when the atoms start in a singly excited state; although this does not correspond to a physical situation, it gives insight into some of the mechanisms controlling the recoil of the atoms. Section IV contains the results for a laser pulse interacting with a grid of atoms; the recoil varies for changing atomic spacing for a fixed detuning as well as for a fixed spacing and a variable detuning.

II. METHODS

The calculations described below are for the recoil of atoms due to the absorption and reemission of photons. The atoms are either in a line or in a 2D array in a plane. The number of atoms will be denoted by N. To pick a specific geometry, the direction of the initial photon propagation will be in the $\hat{y}$ direction, $\mathbf{k}_0 = k\hat{\mathbf{y}}$, with the polarization in the z direction, $\hat{\mathbf{E}} = \hat{\mathbf{z}}$. Boldface type will indicate vectors while $\hat{\mathbf{z}}$ is a unit vector. The vector $\mathbf{r}_j$ is the position of atom j and not an internal, electronic, degree of freedom.

The calculation of the recoil is performed using density matrix techniques. Generically, the density matrix is a solution of the master equation [13,17,18,38,41]

$$\frac{\partial \rho}{\partial t} = \frac{1}{i\hbar}[H, \rho] + \mathcal{L}(\rho), \tag{1}$$

where the ρ is the density matrix, H is an effective Hamiltonian, and $\mathcal{L}$ is the Lindblad superoperator. The Hamiltonian and Lindblad superoperator will be given below. They both contain terms from the dipole field propagator. The difference between the positions of two atoms occurs many times below so we will introduce the definitions

$$\mathbf{r}_{ij} \equiv \mathbf{r}_i - \mathbf{r}_j, \qquad \mathbf{r}'_{ij} \equiv \mathbf{r}_i - \mathbf{r}'_j, \qquad \mathbf{r}''_{ij} \equiv \mathbf{r}'_i - \mathbf{r}'_j \tag{2}$$

to simplify the notation.

The goal of this paper is to calculate the effects from recoil numerically with as few approximations as possible. However, for more than a couple of atoms, the dimension of ρ becomes too large to treat numerically for typical atoms. Instead of approximating the results from Eq. (1), we will simplify the internal states of the atom to reduce the size of the density matrix in the calculations. There could be important effects missed due to the simplification but the basic phenomena should be preserved.

One of the simplifications is to simulate the case where there is one ground state and one excited state. This simplification is often used in calculations because the ground electronic state of a many atom system is only one state. By also restricting the excited level to one state, the number of states increases most slowly with the number of atoms. In the calculations below, the formulas will be for a system where the ground state has zero angular momentum and the excited state has one unit of angular momentum. The other simplification will be to restrict the system to the weak laser limit so that only the ground state and singly excited states are relevant. This limitation is to match the simulations of Refs. [16,17,24] and to reduce the effects from other processes (e.g., having a pair of excitations on neighboring atoms).

Because we are simulating 0–1 transitions in the weak laser limit, the internal states of each atom can be treated as harmonic oscillators instead of the two-state system used below: the resulting equations below for the density matrix and recoil momentum and energy would be unchanged if the internal states are treated as harmonic oscillators.

The density matrix will be used to represent both the internal states of the atom and the positional degrees of freedom. Since there are only 0 or 1 excited atom at a time, the collective internal states will be represented using the simplified notation: the ground state corresponds to all atoms

in the electronic ground state, $|g\rangle = |g_1 g_2 \dots g_N\rangle$, while the N different singly excited states are $|e_i\rangle = |g_1 g_2 \dots e_i \dots g_N\rangle$. The position terms in the density matrix will be represented using the atoms' coordinates $\mathbf{r}_i$. The full density matrix will be represented as

$$\begin{aligned}\rho = {} & |g\rangle\langle g|\rho_{gg}(\mathbf{r}_1, \mathbf{r}_2, \dots \mathbf{r}_N; \mathbf{r}'_1, \mathbf{r}'_2, \dots \mathbf{r}'_N) \\ & + \sum_i |e_i\rangle\langle g|\rho_{e_i g}(\mathbf{r}_1, \mathbf{r}_2, \dots \mathbf{r}_N; \mathbf{r}'_1, \mathbf{r}'_2, \dots \mathbf{r}'_N) \\ & + \sum_i |g\rangle\langle e_i|\rho_{g e_i}(\mathbf{r}_1, \mathbf{r}_2, \dots \mathbf{r}_N; \mathbf{r}'_1, \mathbf{r}'_2, \dots \mathbf{r}'_N) \\ & + \sum_{ij} |e_j\rangle\langle e_i|\rho_{e_j e_i}(\mathbf{r}_1, \mathbf{r}_2, \dots \mathbf{r}_N; \mathbf{r}'_1, \mathbf{r}'_2, \dots \mathbf{r}'_N) \quad (3)\end{aligned}$$

with the ρ_{ab} functions of $6N$ variables representing the position components of the density matrix.

The effective Hamiltonian, H, is the sum of three distinct types of terms: (i) the trapping Hamiltonian for each atom; (ii) the laser-atom interaction; and (iii) the dipole-dipole interaction between an excited and a ground-state atom. The Hamiltonian will be in the rotating wave approximation so that the fast time dependence from the oscillation of the electric field is removed. The trapping Hamiltonian for each atom will be assumed to be deep enough that it can be approximated as a simple harmonic oscillator for each atom, leading to

$$\begin{aligned}H_t &= \sum_j \left[\frac{\mathbf{p}_j^2}{2M} + V(\mathbf{r}_j - \mathbf{R}_j)\right] \\ V(\mathbf{r}) &= \frac{1}{2}M\left[\omega_\perp^2 x^2 + \omega_\parallel^2 y^2 + \omega_\perp^2 z^2\right], \quad (4)\end{aligned}$$

where the x, z harmonic oscillator frequency is assumed to be the same while that in y is different and $\mathbf{R}_i$ is the average position of the ith atom. To isolate the effects from recoil, we have chosen to have the ground and excited states experience the same trapping potential, i.e., the atoms are trapped at the magic wavelength. The laser-atom term will include the effect from the detuning as well as the laser-atom interaction:

$$H_l = \hbar \sum_j \left[-\delta \pi_j^\dagger \pi_j + \frac{\Omega}{2}\pi_j^\dagger e^{i\mathbf{k}_0\cdot\mathbf{r}_j} + \frac{\Omega^*}{2}\pi_j e^{-i\mathbf{k}_0\cdot\mathbf{r}_j}\right], \quad (5)$$

where $\pi_j = |g_j\rangle\langle e_j|$ is the lowering operator for the internal state of atom j, Ω is the Rabi frequency, δ is the detuning, and $\mathbf{k}_0 = k\hat{\mathbf{y}}$ is the initial wave number of the photons. The dipole-dipole interaction term is

$$H_{dd} = \hbar \sum_{j\neq i} \mathrm{Im}[g(\mathbf{r}_{ji})]\pi_j^\dagger \pi_i, \quad (6)$$

where $\mathrm{Im}[\alpha]$ means take the imaginary part of α and we used Eq. (2). For z polarization of the excitation

$$g(\mathbf{r}) = \frac{\Gamma}{2}\left[P_0(\cos\theta)h_0^{(1)}(kr) + P_2(\cos\theta)h_2^{(1)}(kr)\right], \quad (7)$$

where P_ℓ are the Legendre polynomials, $h_\ell^{(1)}$ are the outgoing wave spherical Hankel functions, $\cos\theta = z/r$, and Γ is the radiative decay rate of the excited state. Lastly, the Lindblad term is equal to

$$\begin{aligned}\mathcal{L}(\rho) = \sum_{i,j} & [2\mathrm{Re}[g(\mathbf{r}'_{ji})]\pi_j \rho \pi_i^\dagger - \mathrm{Re}[g(\mathbf{r}_{ij})]\pi_i^\dagger \pi_j \rho \\ & - \mathrm{Re}[g(\mathbf{r}''_{ij})]\rho \pi_i^\dagger \pi_j], \quad (8)\end{aligned}$$

where $\mathrm{Re}[\alpha]$ means take the real part of α and we used Eq. (2) $\mathbf{r}'_{ji} = \mathbf{r}_j - \mathbf{r}'_i$, etc. This term includes the usual one atom decay term when $i = j$.

Two important properties will be used extensively below. The first is that the $\mathrm{Re}[g(\mathbf{r})]$ is an even function, which means the first derivative in any direction is zero in the limit $\mathbf{r} \to 0$. The other is that $\nabla^2 g(\mathbf{r}) = -k^2 g(\mathbf{r})$ because the g is the sum of solutions of the Helmholtz equation.

A. Slow oscillation approximation

Besides the simplifications described above, there will be one approximation in the solution of the master equation. The calculations will only be for situations where the time scale of the atom motion is much slower than the time evolution of the internal states. Thus, the calculations will be for cases where $\Gamma \gg \omega_\perp, \omega_\parallel$ and where the laser pulse has a time width much shorter than the periods. In practice, this situation will often occur since the frequencies are typically less than a few 10's of kHz while the excited-state decay rates are often larger than 10^6 s^{-1}. The restriction on the laser pulse duration implies it is less than a few μs.

Within this approximation, the H_t part of the Hamiltonian has hardly any effect while the internal states are excited and then decay back to the ground state. As will be seen below, this leads to the density matrix after the excited states have all decayed, but before the time scale of the atom trap, having a spatial dependence with the form

$$\begin{aligned}\rho_f(\mathbf{r}_1, \mathbf{r}_2 \dots; \mathbf{r}'_1, \mathbf{r}'_2 \dots) = {} & \rho_0(\mathbf{r}_1, \mathbf{r}_2 \dots; \mathbf{r}'_1, \mathbf{r}'_2 \dots) \\ & \times F(\mathbf{r}_1, \mathbf{r}_2 \dots; \mathbf{r}'_1, \mathbf{r}'_2 \dots), \quad (9)\end{aligned}$$

where ρ_0 is the initial spatial dependence and F is a function with the property

$$F(\mathbf{r}_1, \mathbf{r}_2 \dots; \mathbf{r}_1, \mathbf{r}_2 \dots) = 1 \quad (10)$$

to preserve the norm of the density matrix. The function F does not necessarily have unit norm except for the case of Eq. (10). Lastly, F is Hermitian: $F(\mathbf{r}; \mathbf{r}') = F^*(\mathbf{r}'; \mathbf{r})$ where $\mathbf{r}$ represents all of the coordinates.

The physical parameters discussed below will be the recoil momentum and the recoil energy of the different atoms; said differently, these are the change in momentum and energy. They are computed from the proportionality function, F. The simplest case is the change in momentum, which can be obtained by using the product rule of calculus. The expectation value of the jth momentum just after the atoms have returned to the ground state is

$$\begin{aligned}\langle \mathbf{p}_j \rangle_f &= \frac{\hbar}{i}\int [\nabla_j(\rho_0 F)]\delta(\mathbf{r}'_{11})\delta(\mathbf{r}'_{22}) \dots d^3 r_1 d^3 r'_1 d^3 r_2 d^3 r'_2 \dots \\ &= \langle \mathbf{p}_j \rangle_0 + \Delta \mathbf{p}_j, \quad (11)\end{aligned}$$

where $\nabla_j = \hat{\mathbf{x}}\partial/\partial x_j + \hat{\mathbf{y}}\partial/\partial y_j + \hat{\mathbf{z}}\partial/\partial z_j$, the first term is derived from Eq. (10), and is the original expectation value of

the momentum and the second term is a definition but is physically the change in the expectation value of the momentum (i.e., the recoil momentum):

$$\Delta \mathbf{p}_j = \frac{\hbar}{i}\int [\rho_0(\nabla_j F)]\delta(\mathbf{r}'_{11})\delta(\mathbf{r}'_{22})\ldots d^3r_1 d^3r'_1 d^3r_2 d^3r'_2\ldots \equiv \mathrm{Tr}[(\mathbf{p}_j F)\rho_0]. \quad (12)$$

In the cases treated below, the $\langle \mathbf{p}_j\rangle_0 = 0$ because the initial state will be a thermal, trapped state, which must have expectation value of zero for the momentum.

In a similar way the change in the expectation value of the motional energy can be computed from the kinetic energy since the time scale of the trap is slow. Defining the kinetic energy operator of the jth atom as $K_j = \mathbf{p}_j^2/(2M)$, the expectation value of the kinetic energy of the jth atom just after the atoms have returned to the ground state can be obtained from the product rule and is

$$\langle K_j\rangle_f = \frac{\hbar^2}{2M}\mathrm{Tr}[\nabla_j\cdot\nabla'_j(\rho_0 F)] \equiv \langle K_j\rangle_0 + \Delta K_j, \quad (13)$$

where the first term is derived from Eq. (10) and is the original expectation value of the kinetic energy and the last term is the change in the kinetic energy. Because we are starting from a thermal state or the ground state, the cross derivative terms (one derivative on ρ_0 and one on F) are exactly 0 because, for example, $\partial\rho_0/\partial x_j = \partial\rho_0/\partial x'_j$ after setting all $\mathbf{r}_j = \mathbf{r}'_j$ while $\partial F/\partial x'_j = \partial F^*/\partial x_j = -\partial F/\partial x_j$ since $\partial F/\partial x_j$ is purely imaginary after setting all $\mathbf{r}_j = \mathbf{r}'_j$. Thus, for this initial configuration

$$\Delta K_j = \frac{\hbar^2}{2M}\int [\rho_0(\nabla_j\cdot\nabla'_j F)]\delta(\mathbf{r}'_{11})\delta(\mathbf{r}'_{22})\ldots d^3r_1 d^3r'_1\ldots = \mathrm{Re}[\mathrm{Tr}[(K_j F)\rho_0]], \quad (14)$$

where ∇'_j is the derivative with respect to the primed coordinate and we have used $(\nabla_j\cdot\nabla'_j F) = -\mathrm{Re}[\nabla_j^2 F]$; this relation can be derived for any function with the property $F(\mathbf{r}_j,\mathbf{r}'_j) = F^*(\mathbf{r}'_j,\mathbf{r}_j)$.

In most cases, the derivatives were computed using simple two- or three-point difference expressions with the point separation a small fraction of a wavelength of light. Convergence was checked by comparing the results for different step sizes.

III. SINGLY EXCITED, COHERENT DECAY

The case of laser excitation followed by emission of a photon is complicated by the role played by the laser-atom interaction. There is a different amount of recoil depending on the strength, the duration, and the detuning of the laser. In order to more simply understand how the atom recoil depends on the separation and placement of the atoms, this section will describe results for the simplified situation where there is no laser but the system starts with one atom excited.

Section IV will treat the more physical case where the atoms start in the ground state then a laser pulse causes an excitation followed by photon emission to the ground state.

A. One atom

This section treats the simplest possible case, i.e., where there is only one atom. Thus, not only is there no laser-atom interaction, there is also no dipole-dipole interaction between atoms. It is worth presenting the derivation for this case since the results are analytically known but it also shows how the recoil energy is incorporated using the master equation.

For this case, the master equation reduces to the uncoupled equations

$$\frac{\partial\rho_{ee}(\mathbf{r}_1,\mathbf{r}'_1,t)}{\partial t} = -\Gamma\rho_{ee}(\mathbf{r}_1,\mathbf{r}'_1,t)$$
$$\frac{\partial\rho_{gg}(\mathbf{r}_1,\mathbf{r}'_1,t)}{\partial t} = 2\mathrm{Re}[g(\mathbf{r}'_{11})]\rho_{ee}(\mathbf{r}_1,\mathbf{r}'_1,t), \quad (15)$$

where the identity $\mathrm{Re}[g(\mathbf{r}_1-\mathbf{r}'_1)]\to\Gamma/2$ as $\mathbf{r}'_1\to\mathbf{r}_1$ was used in the first equation. At $t=0$, the terms of the density matrix are $\rho_{gg}=0$ and $\rho_{ee}(\mathbf{r}_1,\mathbf{r}'_1,0) = \rho_0(\mathbf{r}_1,\mathbf{r}'_1)$ using the notation of Eq. (9). These two equations can be solved analytically for ρ_{ee} and ρ_{gg}. In the limit that the final time is much larger than $1/\Gamma$ but much shorter than the vibrational periods, the $\rho_{ee}\to 0$ and the

$$\rho_f(\mathbf{r}_1,\mathbf{r}'_1) = \frac{2\mathrm{Re}[g(\mathbf{r}'_{11})]}{\Gamma}\rho_0(\mathbf{r}_1,\mathbf{r}'_1) \quad (16)$$

using the notation of Eq. (9), which means $F(\mathbf{r}_1,\mathbf{r}'_1) = 2\mathrm{Re}[g(\mathbf{r}_1-\mathbf{r}'_1)]/\Gamma$.

As asserted above, the $F(\mathbf{r}_1,\mathbf{r}'_1)\to 1$ as $\mathbf{r}'_1\to\mathbf{r}_1$. Having obtained the function F, the change in the expectation value of the momentum can be obtained

$$\Delta\mathbf{p}_1 = \frac{2\hbar}{i\Gamma}\mathrm{Tr}[(\nabla_1\mathrm{Re}[g(\mathbf{r}_1-\mathbf{r}'_1)]\rho_0] = 0 \quad (17)$$

because $\mathrm{Re}[g(\mathbf{r}_1-\mathbf{r}'_1)]$ is an even function of the separation vector. This is expected because, for any emission direction, the photon is equally likely to be emitted in the opposite direction, which means the expectation value should be 0. Similarly, the change in the expectation value of the kinetic energy is

$$\Delta K_1 = \frac{-\hbar^2}{2M}\mathrm{Tr}[(\nabla_1^2 F)\rho_0] = \frac{\hbar^2k^2}{2M}\mathrm{Tr}[F\rho_0] = \frac{\hbar^2k^2}{2M}, \quad (18)$$

where the fact that g is a solution of the Helmholtz equation was used in the first step and the $\mathrm{Tr}[\rho_f]=1$ was used in the second step. This shows that, as expected, the change in kinetic energy is just the recoil energy

$$E_r = \frac{\hbar^2k^2}{2M} \quad (19)$$

from the photon emission.

B. Two atoms

This section will treat in detail the case of two atoms. We will do calculations at two levels of simplification. In the first, the atoms will start in a state where the atoms' internal and positional degrees of freedom are not entangled. In the second, we will include an entanglement that could result from the recoil absorption of a photon.

This section will take advantage of the fact that the Hamiltonian and the Lindblad superoperator commutes with the

swap operator, which exchanges the internal states of the two atoms. For this section, we will use the notation

$$|\pm\rangle \equiv (|e_1\rangle \pm |e_2\rangle)/\sqrt{2}, \tag{20}$$

where, as discussed above, $|e_i\rangle$ is the N-atom state $|g_1 g_2 \ldots e_i \ldots g_N\rangle$; $N = 2$ for this section. We will use these states to define the density matrix. As an example, one of the terms of the density matrix representation Eq. (3) will be $|+\rangle\langle g|\rho_{+g}(\mathbf{r}_1, \mathbf{r}_2; \mathbf{r}'_1, \mathbf{r}'_2)$. Below, we will suppress the explicit writing of the spatial dependence except where confusion might arise.

1. Nonentangled initial state

The initial density matrix will be $\rho = \rho_0|+\rangle\langle+| = \rho_{++}(t=0)|+\rangle\langle+|$. The time-dependent density matrix, Eq. (1), reduces to

$$\begin{aligned}\frac{\partial \rho_{++}}{\partial t} &= -[\Gamma_{++} + i\dot{\Phi}_{++}]\rho_{++} \\ \frac{\partial \rho_{gg}}{\partial t} &= \mathcal{D}_{++}\rho_{++},\end{aligned} \tag{21}$$

where

$$\begin{aligned}\Gamma_{\pm\pm} &\equiv \Gamma \pm \mathrm{Re}[g(\mathbf{r}_{12})] \pm \mathrm{Re}[g(\mathbf{r}''_{12})] \\ \dot{\Phi}_{\pm\pm} &\equiv \pm\mathrm{Im}[g(\mathbf{r}_{12})] \pm \mathrm{Im}[g^*(\mathbf{r}''_{12})] \\ \mathcal{D}_{ss'} &\equiv \mathrm{Re}[g(\mathbf{r}'_{11}) + sg(\mathbf{r}'_{21}) + s'g(\mathbf{r}'_{12}) + ss'g(\mathbf{r}'_{22})],\end{aligned} \tag{22}$$

where $s, s' = \pm$ and the general form will be used in the next section. Note that there is a phase accumulation term, $\dot{\Phi}_{++}$, that arises from the collective Lamb shift between the two atoms due to the dipole-dipole interaction. When $\mathbf{r}''_{12} \to \mathbf{r}_{12}$, the phase accumulation term is 0.

These equations can be solved analytically as in the preceding section and lead to

$$F(\mathbf{r}_1, \mathbf{r}_2; \mathbf{r}'_1, \mathbf{r}'_2) = \frac{\mathcal{D}_{++}}{\Gamma_{++} + i\dot{\Phi}_{++}}, \tag{23}$$

which does have the property $F(\mathbf{r}_1, \mathbf{r}_2; \mathbf{r}_1, \mathbf{r}_2) = 1$ since in this limit $\dot{\Phi}_{++} = 0$ and $\mathcal{D}_{++} = \Gamma_{++} = \Gamma + 2\mathrm{Re}[g(\mathbf{r}_{12})]$. Having derived the expression for F, Eqs. (12) and (14) can be used to find the change in momentum and kinetic energy due to the recoil. As with the one-atom case, the total momentum change must be zero due to the symmetry of photon emission. However, atom 1 can have a nonzero change in momentum that is exactly opposite that of atom 2. The total change in kinetic energy will be nonzero but will not necessarily equal E_r due to the dipole-dipole interactions. The form of F is sufficiently complicated that we numerically evaluated the derivatives in Eqs. (12) and (14).

Figure 2(a) shows the results for the change in kinetic energy as a function of the separation of the atoms when the separation is in the x or z direction. For each direction of separation, calculations are performed for a case where the spatial spread in ρ_0 is much smaller than the wavelength of the photons (red solid for x separation and blue dashed for z separation) and for a thermal distribution (orange short-dashed for x separation and green dotted for z separation). The thermal calculation uses parameters for ^{85}Rb in a trap with frequencies 40, 10, 40 kHz in the x, y, z directions and a temperature of 1 μK [for these frequencies and temperature the $1/e$ length for the density is $(0.51/k, 1.81/k, 0.51/k)$ with $k = 2\pi/\lambda$].

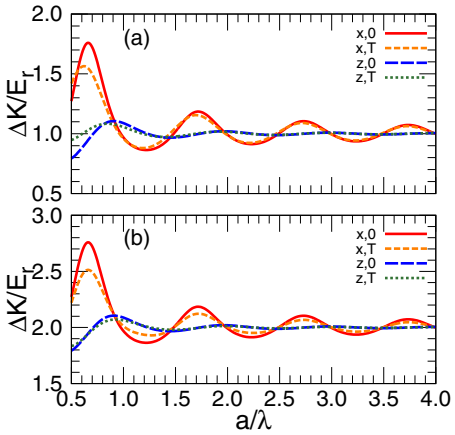

FIG. 2. The total recoil energy, $\Delta K = \Delta K_1 + \Delta K_2$, in units of the recoil energy, E_r, versus the separation, a, of the two atoms in units of the wavelength, λ. In both plots, the excitation is assumed to be for the z component: $J_g = 0, M_g = 0 \to J_e = 1, M_e = 0$. In (a), the initial state is a symmetric, singly excited state, Eq. (20), and (b) has the excitation entangled with a momentum kick, Eq. (24). In both plots, the red solid (blue dashed) line is for separation in the $x(z)$ direction with the initial spatial distribution much smaller than a wavelength and the orange short-dashed (green dotted) line is for separation in the $x(z)$ direction but with a thermal spatial distribution corresponding to 1 μK as described in the text.

There are a number of interesting features for the recoil energy. The first, and most important, is that the change in energy is not E_r. The recoil energy of the pair oscillates around the single-atom value, converging to E_r as the separation, a, gets larger. The size of the oscillation is much different for the case when the separation is perpendicular to the polarization of the internal state (x separation) than when it is parallel (z separation) with the x separation having a much larger oscillation. The difference between the ΔK for the x and z separation is an indication about which processes are important. The reason for the larger ΔK for the x separation is related to the discussion of Fig. 4: the collective decay has a larger effect than the collective Lamb shift on ΔK for this range of a. The collective decay has a smaller effect on the parallel (z) separation compared to the perpendicular (x) separation because photons are emitted perpendicular to the dipole. Another difference is that the perpendicular separation has maxima energy change approximately at integer plus 3/4 wavelength while the parallel separation has maxima energy change approximately at integer wavelengths. Finally, the spread in the atomic positions only has a non-negligible effect when the separation is less than $\sim 0.8\lambda$ and the effect is not qualitative even in the range 0.5–0.8λ. Since the largest averaging occurs in the y direction, this is perhaps not so surprising because the main separation is perpendicular to this.

Mathematically, $\Delta K \neq E_r$ arises due to the denominator of F. Only taking derivatives of the numerator gives $\Delta K = E_r$. The denominator encapsulates two effects: (i) the change

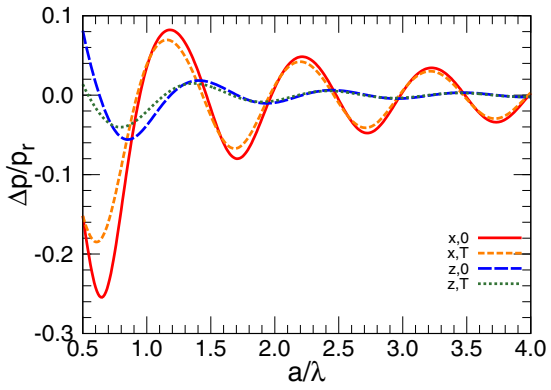

FIG. 3. Same as Fig. 2(a) except all plots are for $\Delta p/p_r$ ($p_r = \hbar k$) for atom 1 in the direction of the atom separation. The line types are the same as for Fig. 2(a).

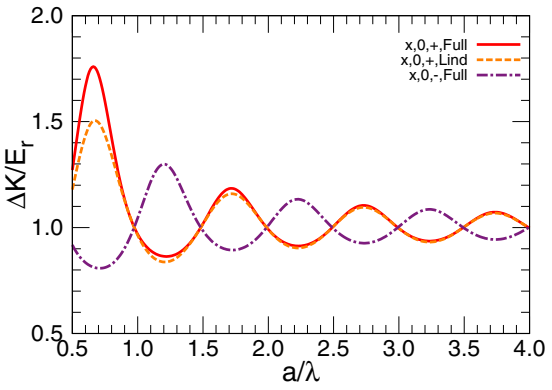

FIG. 4. Same as Fig. 2 except all plots are for separation in the x direction with initial spatial extent for each atom much smaller than a wavelength. The red solid line is the same as Fig 2(a). The orange short-dashed line is the same except that we only keep the Lindblad terms in Eq. (21) which is equivalent to disregarding the potential energy from the dipole-dipole interaction. The purple dash-dotted line is for the full master equation but for an antisymmetric excitation.

in the decay rate due to the interference of photon emission from the two atoms (Γ_{++}) and (ii) the momentum kick due to the spatial dependence of the collective Lamb shift ($\dot{\Phi}_{++}$). Figure 3 shows the change in momentum of atom 1 in the direction of the atom-atom separation (the momentum change perpendicular to the separation is 0). The momentum change of atom 2 is opposite that of atom 1. This change in momentum can only occur due to the collective Lamb shift. It oscillates around 0 with an amplitude that decreases with increasing separation. As with Fig. 2(a), the effect is larger for perpendicular separation and the effect of position averaging is small. Although the momentum change is nonzero, the size of the effect also suggests that the collective Lamb shift is not the main reason for the ΔK oscillation. Estimating ΔK from $2 \times \Delta p^2/(2M)$ would lead to peaks with a separation of $\lambda/2$ not λ as seen in Fig. 2(a). Also the size does not match [for example the Δp peak in the x separation of $\sim 1.2\lambda$ would give $\Delta K \sim 2 \times (0.08 p_r)^2/2M \sim 0.01 E_r$, which is a factor of 20 smaller than the actual change].

Figure 4 compares three calculations for ΔK when the atoms have x separation. The red solid line is the same as for Fig. 2(a). The orange short-dashed line is for a calculation where the $\dot{\Phi}_{++}$ term is artificially set to 0; this is equivalent to getting rid of the collective Lamb shift but keeping the collective decay. Except for the smallest separation, this calculation almost exactly reproduces the full calculation. Even at small separation, 0.5–0.8λ, the difference is more quantitative than qualitative, which suggests that the main effect is due to the collective decay. This is confirmed by comparison with a calculation (purple dash-dot line) where the atoms are initialized to the antisymmetric excited state $\rho_0|-\rangle\langle -|$. At separations where $|+\rangle$ has a larger decay rate, the $|-\rangle$ has a smaller decay rate and vice versa, which is evident in Fig. 4 where the solid red and green dotted lines oscillate around 1 out of phase by 180°. This strongly suggests the collective decay is the main mechanism because it has the same property.

2. *Entangled initial state*

The results of Sec. III B 1 do not account for the momentum kick during photon absorption. To mimic this effect, we performed calculations where the initial electronic state is entangled with a momentum kick:

$$|\psi\rangle = \frac{e^{iky_1}|e_1\rangle + e^{iky_2}|e_2\rangle}{\sqrt{2}} = \alpha_+|+\rangle + \alpha_-|-\rangle, \tag{24}$$

where $\alpha_\pm = [\exp(iky_1) \pm \exp(iky_2)]/2$. The initial density matrix is

$$\rho = \rho_0 \sum_{i,j=\pm} \alpha_i \alpha_j^* |i\rangle\langle j| \equiv \sum_{i,j=\pm} \rho_{ij}|i\rangle\langle j|, \tag{25}$$

where, as described above, we have suppressed the explicit writing of the spatial dependence. Because of the symmetry in the collective Lamb shift and decay terms, the density matrix equations reduce to

$$\begin{aligned} \frac{\partial \rho_{ss'}}{\partial t} &= -[\Gamma_{ss'} + i\dot{\Phi}_{ss'}]\rho_{ss'} \\ \frac{\partial \rho_{gg}}{\partial t} &= \sum_{ss'} \mathcal{D}_{ss'}\rho_{ss'}, \end{aligned} \tag{26}$$

where Eq. (22) has been used. The first equation can be analytically solved and used in the second equation to obtain the final density matrix. This leads to the expression for F being

$$F = \sum_{s,s'} \frac{\mathcal{D}_{ss'}}{\Gamma_{ss'} + i\dot{\Phi}_{ss'}} \alpha_s \alpha_{s'}^*, \tag{27}$$

where the $s, s' = \pm$ and the spatial dependence [see Eqs. (22) and (24)] has been suppressed as discussed above. Note that the result without the absorption kick, Eq. (23), results by setting $\alpha_+ = 1, \alpha_- = 0$.

The change in energy for this case is plotted in Fig. 2(b) for separation in the x and z direction. As with the case with no photon absorption kick, the spatial spread is not a large effect. The dependence on the direction of separation, separation distance, etc. is very similar to the case with no photon kick except that all of the energy changes have increased by another E_r. Perhaps this is not very surprising because

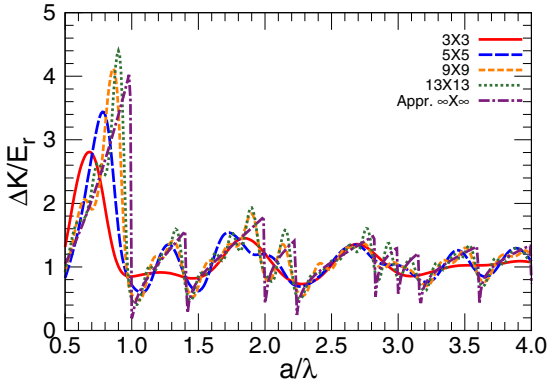

FIG. 5. Same as Fig. 2(a) except for $n \times n$ atoms in a square array with spacing a in the xz plane with the spatial extent of each atom much smaller than λ. The plot is for n^2 times the recoil energy of the center atom. The solid red line is for 3×3, the blue dashed line is for 5×5, the orange short-dashed line is for 9×9, and the green dotted line is for 13×13. The purple dash-dotted line is the approximate $\infty \times \infty$ grid.

the absorption gives a kick in the y direction whereas the emission is mainly averaged over many directions so that the total energy change is the sum of the energies from the two steps.

C. Two-dimensional grid of atoms

References [16,17] calculated the reflection of photons from a plane of equally spaced atoms. To give an idea of the change in energy per photon, we solved Eq. (1) numerically for an $n \times n$ square grid when the initial electronic state is the symmetric state $[|e_1\rangle + |e_2\rangle + \ldots]/\sqrt{N}$. The change in energy for a finite grid does not have a simple analytic form because the dipole-dipole interaction does not give pure decay due to the edges of the grid. In all of the calculations, we treat the case where the spatial distribution of atoms is much smaller than a wavelength because the multidimensional integrations become very time consuming. From the two-atom calculations, we know that this will give results in qualitative agreement with a spatial average as long as the x, z extent is small.

To get an idea of how much energy each photon deposits in the lattice, we computed the recoil energy of the center atom and multiplied that result by $N = n^2$. This should more quickly converge to the infinite lattice result with increasing n because this atom is furthest from the edges of the grid. The results are shown in Fig. 5 for different grid sizes. The atoms are on a square array in the xz plane. As with the two atom case, the recoil energy varies around $\Delta K \sim E_r$ and is closer to that value for larger separations. As expected, the oscillations become sharper with increasing n because the superradiance and subradiance effects become larger. One interesting feature is that the recoil energy can be larger than $4E_r$ for large grids, which indicates that reflecting photons from a large grid might result in relatively large recoil energy per photon.

The infinite lattice with atoms starting in the symmetric excited state can be approximately solved analytically because the terms in the density matrix equation mainly couple the symmetric excited state and the ground state; when the atoms are not on a perfect lattice (as when computing the derivatives), there is some coupling to the nonsymmetric states. Taking as an approximation only the symmetric excited state and the ground state, the equations for the coefficients of these states are

$$\frac{\partial \rho_{++}}{\partial t} = -\left\{\Gamma + \frac{1}{N}\sum_{j\neq i}[g(\mathbf{r}_{ji}) + g^*(\mathbf{r}'_{ji})]\right\}\rho_{++}$$
$$\frac{\partial \rho_{gg}}{\partial t} = \frac{1}{N}\sum_{j,i} 2\mathrm{Re}[g(\mathbf{r}'_{ji})]\rho_{++}, \tag{28}$$

where the limit $N \to \infty$ is taken. As above, these equations are solved by writing the ρ_{++} as an exponential function of time and then integrating the second equation. In this case, every atom has the same change in kinetic energy so the energy given to the grid of atoms is $N\times$ that of atom 1. After some manipulations, it can be shown that the energy given to the grid for this case is

$$\Delta K_\infty = E_r \frac{\sum_{j=1}^{\infty} 2\mathrm{Re}[g(\mathbf{r}_{1,j}]}{\Gamma + \sum_{j=2}^{\infty} 2\mathrm{Re}[g(\mathbf{r}_{1,j}]}, \tag{29}$$

where we chose atom 1 to be the reference atom but the result does not depend on this choice. The purple dash-dot line in Fig. 5 shows this result. It is clear that the numerical results are converging to the ∞ grid case as more atoms are added. The sharp variation are when the separation of atoms give collective emission in the plane: $a = 1, \sqrt{2}, 2, \sqrt{3}, \ldots, \times\lambda$.

IV. EXCITATION BY LASER PULSE

In this section, we perform calculations where the atoms start in the ground state, a laser pulse excites the atoms to a singly excited state (at most), and then the atoms decay back to the ground state. All of the calculations in this section will be for a square array of $n \times n$ atoms to gain insight into the simulations of Refs. [16,17]. As with Sec. III C, the calculations are limited to the case where the spatial extent of the wave function is much smaller than λ, and we will compute the recoil for the center atom and multiply by N to avoid some of the effects from the grid edge. At the end of the calculation, we numerically calculate the derivatives needed to obtain the recoil momentum and energy. Because there is not a general way to solve for this case analytically, this section is mostly the description of numerical results.

The calculations are for a time-dependent laser amplitude

$$\Omega(t) = \Omega_0 e^{-t^2/t_w^2}, \tag{30}$$

where the Ω_0 was chosen to be a small value, $\Gamma/400$. In this limit, the recoil energy is proportional to Ω_0^2. The recoil energy depends on the duration of the laser pulse in a nontrivial way. For small t_w compared to $1/\Gamma$, the excitation is an impulsive step and leads to a state, just after the laser pulse is finished, that is a good approximation to the entangled excitation state

$$|\psi\rangle_0 = \sqrt{1 - |C|^2}|g\rangle + C|+\rangle_{n\times n}, \tag{31}$$

where $|+\rangle_{n\times n} = \sum_j |e_j\rangle \exp(iky_j)/\sqrt{N}$. In this limit, C is proportional to $t_w\Omega_0$. This is reminiscent of the entangled

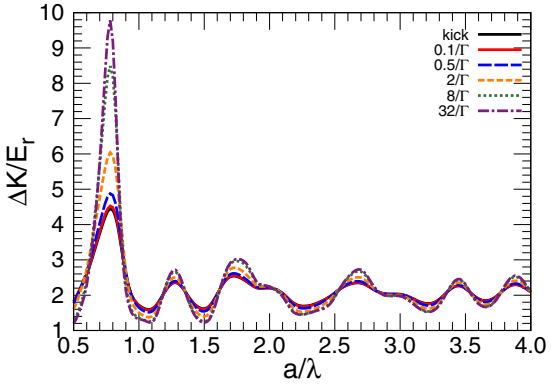

FIG. 6. The energy recoil (times 25) of the center atom of a 5×5 square grid versus the atom separation for various time width of the laser pulse. The black solid line (which can hardly be seen because the red solid line overlays it) is for the case of no laser but with the initial wave function a singly excited state entangled with the momentum kick, $|+\rangle_{n\times n}$ of Eq. (31). In units of $1/\Gamma$, the solid red line is for $t_w = 0.1$, the dashed blue line is for 0.5, the orange short-dashed line is for 2, the green dotted line is for 8, and the purple dash-dot line is for 32. All of the lines for laser excitation have been normalized to be the same value at $a = 4\lambda$ as described in the text.

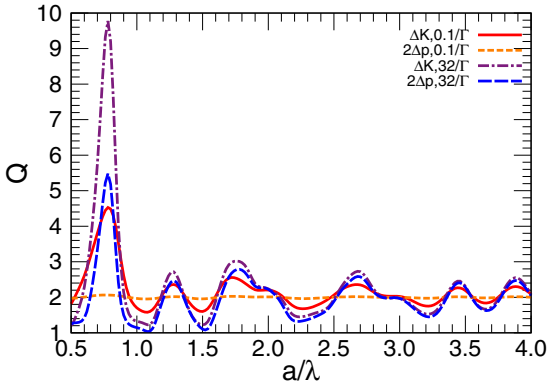

FIG. 7. Same as Fig. 6 for the recoil energy: $Q = 25\beta\Delta K/E_r$ for the middle atom and β is the normalization constant discussed in the caption of Fig. 6. The red solid line ($0.1/\Gamma$) and purple dash-dot line ($32/\Gamma$) are the same as Fig. 6. The orange short-dashed line ($0.1/\Gamma$) and blue dashed line ($32/\Gamma$) are $2\times$ the recoil momentum: $Q = 2 \times 25\beta\Delta p/p_r$.

starting condition above, Eq. (24), so as a comparison we also performed calculations with no laser excitation but with an initial state equaling $|+\rangle_{n\times n}$.

Figure 6 shows the weighted recoil of the center atom (the recoil multiplied by N) versus the separation of the atoms for various laser durations. The detuning for this calculation is 0. Also plotted is the recoil energy for the case of no laser excitation but starting from the entangled state $|+\rangle_{n\times n}$, black solid line. Because the amount of recoil depends on the laser parameters (duration, strength, and detuning), we have normalized all curves to have the same value as the entangled calculation at $a = 4\lambda$. The results for the shortest duration laser pulse, $t_w = 0.1/\Gamma$ red solid line, is nearly indistinguishable from the calculation with no laser but starting from the entangled state, which shows that Eq. (31) is a good approximation for short laser pulses for all separations. This figure also shows that the calculations of Sec. III C qualitatively reproduce the physical case when the separation is more than $\sim\lambda$. However, the level of agreement at smaller separation decreases as the duration of the laser increases beyond $\sim 1/\Gamma$. The fact that the plotted value goes well above 5 for smaller separations is an artifact of the normalization of all curves at $a = 4\lambda$. The sharp increase is more related to the changing line width and shift of the resonance with a.

A different but similar type plot is shown in Fig. 7. In this figure, both the recoil momentum in the y direction as well as the recoil energy are plotted for the shortest and longest laser pulses in Fig. 6 (i.e., $t_w = 0.1/\Gamma$ and $32/\Gamma$). In these plots, we have performed the same normalization of the curves as in Fig. 6 for the recoil energy and the detuning is again 0. For the recoil momentum, we performed the same normalization and scaled by the photon momentum, $\hbar k$, but also multiplied by 2 so that the asymptotic value, $a \to \infty$, goes to 2 for both momentum and energy. The red solid line and purple dash-dot line are the recoil energies from Fig. 6 for $0.1/\Gamma$ and $32/\Gamma$. The orange short-dashed line is the recoil momentum (times 2) for $0.1/\Gamma$. Note that there is almost no variation with a because a photon is equally likely to be absorbed for any separation due to the large laser line width. Also note that the plotted value is roughly 2, which means that every photon delivers a recoil momentum $\simeq \hbar k\hat{y}$ to the grid of atoms. This result could be anticipated because every absorbed photon delivers $\hbar k\hat{y}$ but the emitted photon has symmetrical emission, which does not contribute to the average atomic momentum. When the laser has a long duration, the laser line width becomes narrow; the shifting resonance (due to the collective Lamb shift) and the changing resonance width leads to a strong variation with a. Note that the large increase in recoil energy is at the same separation, $a \sim 0.8\lambda$, where the recoil momentum, blue dashed line, has a large increase. This suggests that a large part of the increases might be due to an enhanced reflectivity of the atom array.

The near unity reflection [16,17] for the atomic array occurs for separations less than a wavelength and for laser pulses with line widths much less than Γ. Because the atom separation is less than a wavelength, a photon with normal incidence to the grid must deliver a recoil momentum of $2p_r\hat{y}$ when it is reflected and 0 when it is transmitted [17]. For every photon through an area a^2, a simple model of the reflection gives a recoil momentum in the y direction of $R \times 2p_r$ where R is the reflection probability. It would also have a recoil energy of $R \times 4E_r$ if each atom independently reflects the photon. The reflection probability for a photon normally incident on an infinite array was given in Ref. [17] and we will compare our numerical results to this idealized case. To gain some understanding of this system, we simulated the case where an $n \times n$ grid has a laser pulse with $t_w = 32/\Gamma$ normally incident on the grid. We performed the calculation with $\Omega = \Gamma/400$ to stay in the single excitation regime for lattices up to 11×11.

When using the form for the laser pulse, Eq. (30), the number of photons incident on an area a^2 can be computed. This is accomplished by integrating the intensity of the laser pulse over time, multiplying by the area a^2, and dividing by

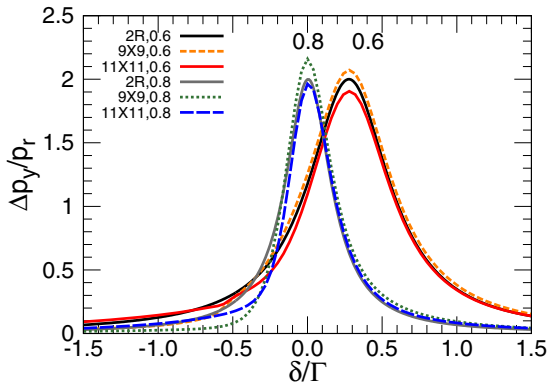

FIG. 8. Recoil momentum for the center atom versus detuning. The recoil momentum is calculated per photon incident on an area a^2, Eq. (32), for a separation of 0.6λ and 0.8λ. The red solid and blue dashed lines are for an 11×11 grid while the orange short-dashed and green dotted lines are for 9×9. The black and gray curves are $2\times$ the reflection probability for a photon normally incident on an infinite array using the results from Ref. [17].

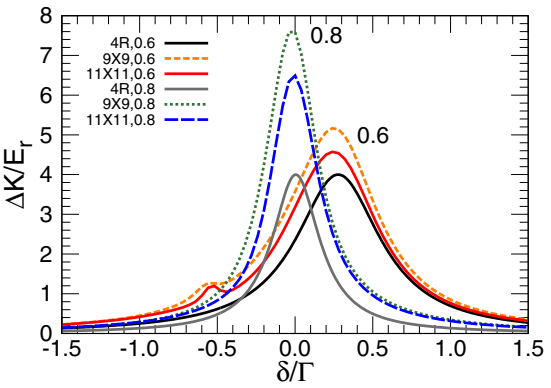

FIG. 9. Recoil energy for the center atom versus detuning. The recoil energy is calculated per photon incident on an area a^2, Eq. (32), for a separation of 0.6λ and 0.8λ. The line types are the same as Fig. 8 except the black and gray curves are $4\times$ the reflection probability for a photon normally incident on an infinite array using the results from Ref. [17].

a photon energy $hf = hc/\lambda$. The number of photons incident on an area containing one atom is

$$\nu = \frac{(2\pi)^{3/2}}{6}(t_w\Gamma)\left(\frac{a}{\lambda}\right)^2\left(\frac{\Omega_0}{\Gamma}\right)^2, \tag{32}$$

where we have grouped products that give dimensionless variables. In the plots, we divide the recoil momentum and recoil energy of the center atom by this photon number to get a value, which is the recoil per incident photon.

Figure 8 shows the plot of the recoil momentum versus detuning of the photon. The calculation is for the center atom in an $n \times n$ array with the recoil momentum divided by the number of photons incident on a unit area, Eq. (32). The plots are for a spacing $a = 0.6\lambda$ and 0.8λ for two array sizes, 9×9 and 11×11. The width and detuning of the resonance changes with the atom spacing. The black and gray lines are $2R$ as calculated for an infinite array [17]. These lines are from a numerical implementation of the full equations in Ref. [17] of the reflection versus detuning for a separation a and has negligible errors. Although the numerical results are not exactly the same as the reflection probability from Ref. [17], they are fairly close in detuning and linewidth. This shows that the basic picture of photons reflecting from the array behaves as expected with respect to the recoil momentum.

Figure 9 shows the plot of the recoil energy versus detuning of the photon. For this calculation, the recoil energy is compared to $R \times 4E_r$, which would be the result if each atom individually reflects a photon. Unlike the recoil momentum, there is a substantial difference in the recoil energy. It is interesting that the effect is much larger for the narrower line ($a = 0.8\lambda$). This effect would be nontrivial for an estimate of the energy deposited in the grid of atoms per reflected photon. For the $a = 0.8\lambda$ case with a 9×9 grid, the center atom gets a recoil energy approximately $2\times$ greater than expected from simple considerations.

V. SUMMARY

Results were presented from calculations of the recoil momentum and energy for photons scattering from an array of atoms. When the atoms are in an array and their separation is comparable to a wavelength of light, the dipole-dipole interaction between the atoms lead to collective scattering. In this case, there can be enhanced optical cross sections, cooperative resonances, chiral quantum optics, etc. The results from the calculations above give insight into how energy might be deposited into the atomic array.

Calculations were performed for the artificial case where the atoms start in a coherent, multiatom, singly excited state and the recoil momentum and energy was determined for the atom system after the photon emission. Calculations were performed for a pair of atoms where analytic results can be obtained as well as for $n \times n$ grids. It was found that entangling a momentum kick with the excitation approximately increased the recoil energy by E_r as would be expected for symmetric photon emission. In all of the cases, the recoil energy was substantially changed from E_r depending on the separation and geometry of the atoms.

Calculations were performed for the case where an $n \times n$ grid of atoms start in their ground state and a weak laser pulse is reflected from the grid. When the duration of the pulse is much shorter than the lifetime of the excited state, the recoil energy equals that for the case where the atoms start in a singly excited state with the excitation entangled with a momentum kick. As the duration of the laser becomes longer than the excited state lifetime, the variation of the resonance energy and width with atom separation leads to complicated variation of the recoil energy. The recoil was investigated for the case where perfect reflection is expected. While the recoil momentum was approximately what would be expected ($2\hbar k$ times the reflection probability), the recoil energy could be substantially larger than expected (up to $\sim 2 \times 4E_r$ times the reflection probability) although in many cases it was close to the expected value. This suggests that the collective scattering

can lead to anomalously larger recoil energies, which might negatively affect the utility of these atomic arrays.

Other arrays of objects can interact collectively with light (for one example from this extensive literature, see Ref. [43]), which raises the question of the recoil energy and/or momentum of each object. There are properties of such arrays, besides being fixed in space, which suggest the features discussed above may not be directly relevant. For example, the calculations above are for the case where there is no dissipation into other modes whereas this is always present to some extent in metamaterial arrays. It may be worth a separate study of the recoil energy and momentum of metamaterial arrays to understand the collective scattering process better.

ACKNOWLEDGMENTS

We thank Xiao Wang and Troy Seberson for critical reading an early version of this paper. This work was supported by the National Science Foundation under Award No. 1804026-PHY. This research was supported in part through computational resources provided by Information Technology at Purdue University, West Lafayette, Indiana.

[1] R. H. Dicke, Phys. Rev. **93**, 99 (1954).
[2] N. E. Rehler and J. H. Eberly, Phys. Rev. A **3**, 1735 (1971).
[3] R. Friedberg, S. R. Hartmann, and J. T. Manassah, Phys. Rep. **7**, 101 (1973).
[4] N. Skribanowitz, I. P. Herman, J. C. MacGillivray, and M. S. Feld, Phys. Rev. Lett. **30**, 309 (1973).
[5] M. Gross, C. Fabre, P. Pillet, and S. Haroche, Phys. Rev. Lett. **36**, 1035 (1976).
[6] M. O. Scully, Phys. Rev. Lett. **102**, 143601 (2009).
[7] Z. Meir, O. Schwartz, E. Shahmoon, D. Oron, and R. Ozeri, Phys. Rev. Lett. **113**, 193002 (2014).
[8] J. Pellegrino, R. Bourgain, S. Jennewein, Y. R. P. Sortais, A. Browaeys, S. D. Jenkins, and J. Ruostekoski, Phys. Rev. Lett. **113**, 133602 (2014).
[9] A. Browaeys, D. Barredo, and T. Lahaye, J. Phys. B **49**, 152001 (2016).
[10] S. L. Bromley, B. Zhu, M. Bishof, X. Zhang, T. Bothwell, J. Schachenmayer, T. L. Nicholson, R. Kaiser, S. F. Yelin, M. D. Lukin, A. M. Rey, and J. Ye, Nat. Commun. **7**, 11039 (2016).
[11] R. J. Bettles, S. A. Gardiner, and C. S. Adams, Phys. Rev. A **92**, 063822 (2015).
[12] D. Plankensteiner, C. Sommer, H. Ritsch, and C. Genes, Phys. Rev. Lett. **119**, 093601 (2017).
[13] S. Jennewein, L. Brossard, Y. R. P. Sortais, A. Browaeys, P. Cheinet, J. Robert, and P. Pillet, Phys. Rev. A **97**, 053816 (2018).
[14] L. F. Buchmann, K. Mølmer, and D. Petrosyan, Phys. Rev. A **95**, 013403 (2017).
[15] Y. Wang, X. Zhang, T. A. Corcovilos, A. Kumar, and D. S. Weiss, Phys. Rev. Lett. **115**, 043003 (2015).
[16] R. J. Bettles, S. A. Gardiner, and C. S. Adams, Phys. Rev. Lett. **116**, 103602 (2016).
[17] E. Shahmoon, D. S. Wild, M. D. Lukin, and S. F. Yelin, Phys. Rev. Lett. **118**, 113601 (2017).
[18] J. P. Clemens, L. Horvath, B. C. Sanders, and H. J. Carmichael, Phys. Rev. A **68**, 023809 (2003).
[19] B. Yan, S. A. Moses, B. Gadway, J. P. Covey, K. R. Hazzard, A. M. Rey, D. S. Jin, and J. Ye, Nature (London) **501**, 521 (2013).
[20] V. Mkhitaryan, L. Meng, A. Marini, and F. J. G. de Abajo, Phys. Rev. Lett. **121**, 163602 (2018).
[21] T. Xia, M. Lichtman, K. Maller, A. W. Carr, M. J. Piotrowicz, L. Isenhower, and M. Saffman, Phys. Rev. Lett. **114**, 100503 (2015).
[22] K. M. Maller, M. T. Lichtman, T. Xia, Y. Sun, M. J. Piotrowicz, A. W. Carr, L. Isenhower, and M. Saffman, Phys. Rev. A **92**, 022336 (2015).
[23] Y. Wang, A. Kumar, T.-Y. Wu, and D. S. Weiss, Science **352**, 1562 (2016).
[24] A. Grankin, P. O. Guimond, D. V. Vasilyev, B. Vermersch, and P. Zoller, Phys. Rev. A **98**, 043825 (2018).
[25] Q. Li, D. Xu, C. Cai, and C. Sun, Sci. Rep. **3**, 3144 (2013).
[26] M. M. Cola, D. Bigerni, and N. Piovella, Phys. Rev. A **79**, 053622 (2009).
[27] J. Guo, P. R. Berman, B. Dubetsky, and G. Grynberg, Phys. Rev. A **46**, 1426 (1992).
[28] J. Javaloyes, M. Perrin, G.-L. Lippi, and A. Politi, Phys. Rev. A **70**, 023405 (2004).
[29] R. Bonifacio and L. De Salvo, Nucl. Instrum. Methods Phys. Res., Sect. A **341**, 360 (1994).
[30] N. Piovella, M. Gatelli, and R. Bonifacio, Opt. Commun. **194**, 167 (2001).
[31] P. Domokos and H. Ritsch, Phys. Rev. Lett. **89**, 253003 (2002).
[32] A. T. Black, H. W. Chan, and V. Vuletić, Phys. Rev. Lett. **91**, 203001 (2003).
[33] K. J. Arnold, M. P. Baden, and M. D. Barrett, Phys. Rev. Lett. **109**, 153002 (2012).
[34] G. Labeyrie, E. Tesio, P. M. Gomes, G.-L. Oppo, W. J. Firth, G. R. Robb, A. S. Arnold, R. Kaiser, and T. Ackemann, Nat. Photon. **8**, 321 (2014).
[35] D. Holzmann, M. Sonnleitner, and H. Ritsch, Eur. Phys. J. D **68**, 352 (2014).
[36] T. Bienaime, M. Petruzzo, D. Bigerni, N. Piovella, and R. Kaiser, J. Mod. Opt. **58**, 1942 (2011).
[37] P. W. Courteille, S. Bux, E. Lucioni, K. Lauber, T. Bienaime, R. Kaiser, and N. Piovella, Eur. Phys. J. D **58**, 69 (2010).
[38] F. Damanet, D. Braun, and J. Martin, Phys. Rev. A **93**, 022124 (2016).
[39] J. D. Miller, R. A. Cline, and D. J. Heinzen, Phys. Rev. A **47**, R4567 (1993).
[40] S. Wolf, S. J. Oliver, and D. S. Weiss, Phys. Rev. Lett. **85**, 4249 (2000).
[41] E. Shahmoon, M. D. Lukin, and S. F. Yelin, *Advances in Atomic, Molecular, and Optical Physics* (Elsevier, New York, 2019), Vol. 68, Chap. 6.
[42] E. Shahmoon, M. D. Lukin, and S. F. Yelin, arXiv:1810.01052.
[43] S. D. Jenkins and J. Ruostekoski, Phys. Rev. Lett. **111**, 147401 (2013).